ISSN: 0067-2904

Theoretical Study of Positive and Negative Parity Coulomb Transitions in ^{40,48}Ca

Mohammed M. Dhhewy *, *Arkan R. Ridha*
Department of Physics, College of Science, University of Baghdad, Baghdad,Iraq

Received: 1/7/2024 Accepted: 28/1/2025 Published: 30/1/2026

Abstract

The nuclear shell model calculations were performed with effective interaction Hsieh-Wildenthal (HW) and G-matrix PF1, (GXPF1) interactions for ^{40}Ca and ^{48}Ca, respectively. The ^{40}Ca was considered to be consisted of ^{32}S as a core and $1d_{3/2}1f_{7/2}$ subshells as a model space. The ^{48}Ca was considered to be consisted of ^{40}Ca as a core and $1f_{7/2}2p_{3/2}1f_{5/2}$ $2p_{1/2}$ subshells as a model space. The obtained one body-density matrix elements (OBDME) for both interactions for the studied Coulomb transitions: For ^{40}Ca, the three non-normal parity transitions (C3): $0^+ \rightarrow 3_1^-$ $(E_x = 3.74\ MeV)$, $0^+ \rightarrow 3_2^-$ $(E_x = 6.29\ MeV)$ and $0^+ \rightarrow 3_3^-$ $(E_x = 6.59\ MeV)$ and one C5 transitions, $0^+ \rightarrow 5_1^-$ $(E_x = 4.49\ MeV)$. For ^{48}Ca, the two C2 transitions: $0^+ \rightarrow 2_1^+$ $(E_x = 3.841\ MeV)$ and $0^+ \rightarrow 2_2^+$ $(E_x = 9.29 MeV)$ and one C4 transitions $0^+1 \rightarrow 4_2^+$ $(E_x = 6.34\ MeV)$ were used in parallel with the transformed harmonic-oscillator basis to compute charge density, elastic electron scattering differential cross-section and elastic and inelastic Coulomb form factors. Finally, the Bohr-Mottelson (B-M), Tassie (T), and valence (V) models were included in the theoretical calculations for the computed inelastic coulomb form factors.

Keywords: Charge density distributions, electron scattering differential cross section, elastic and inelastic Coulomb form factors, charge rms radii, Energy levels

دراسة نظرية للانتقالات الكولومية ذات التناظر الموجب والسالب في ^{40,48}Ca

محمد محمود ضحيوي *, اركان رفعه رضا
قسم الفيزياء، كلية العلوم، جامعة بغداد، بغداد–العراق

الخلاصة

حسابات انموذج القشرة اجريت باستخدام تفاعل HW وتفاعل GXPF1 على ^{40,48}Ca. الكالسيوم–40 اعتبر بانه مكون من ^{32}S كقلب والقشر الثانوية $1d_{3/2}1f_{7/2}$ كانموذج فضاء. الكالسيوم–48 اعتبر بانه مكون من ^{40}Ca كقلب والقشر الثانوية $1f_{7/2}2p_{3/2}1f_{5/2}$ $2p_{1/2}$ كانموذج فضاء. قيم عناصر مصفوفة الجسيم الواحد المستحصلة لكلا التفاعلين استخدمت بالتوازي مع الدوال الموجية للمتذبذب التوافقي المعدل لحساب توزيعات الكثافة الشحنية والمقطع العرضي التفاضلي للاستطارة الالكترونية وعوامل التشكل الكولومية المرنة غير المرنة. للكالسيوم–40، الانتقالات الكولومية C3 غير الاعتيادية، تمت دراستها للانتقالات: $(E_x = 3.74\ MeV)\ 3_1^- \leftarrow 0^+$، $(E_x = 6.29\ MeV)\ 3_2^- \leftarrow 0^+$، $(E_x = 6.59\ MeV)\ 3_3^- \leftarrow 0^+$ بالإضافة الى الانتقال C5، $(E_x = 4.49\ MeV)\ 5_1^- \leftarrow 0^+$. للكالسيوم–48، للانتقالين C2: $2_1^+ \leftarrow$ $(E_x = 3.841\ MeV)\ 2_2^+ \leftarrow 0^+$، $(E_x = 9.29 MeV)\ 0^+$ بالإضافة الى الانتقال C4،

*Email: mohammed.ma@sc.uobaghdad.edu.iq

$4_2^+ \leftarrow 0^+$ $(E_x = 6.34\ MeV)$ تمت دراستها. أخيرا، استقطاب القلب تم ادخاله في الحسابات لحساب
عوامل التشكل الكولومية غير المرنة باستخدام انموذج بور–موتيلسون وانموذج تاسي وانموذج التكافؤ.

1. Introduction

Studying the structure of the nucleus using the electron scattering method has been considering very effective for two reasons. The first reason is that the electron interaction is understood, as the electron interacts with the target's charge and current density electromagnetically. Such interaction is relatively weak; it can be carried out without causing a defect in the structure of the target. The second reason is that the energy lost by the target is fixed, while the momentum transfer (q) can be varied [1, 2]. The theory of calculations for electron scattering off nucleon intensively depend on the opted nuclear wave functions (WF) [1,3]. Such wave functions (WF) must mainly have exponential behavior at large *r*; such exponential behavior plays significant enhancement in the many calculated nuclear properties [4]. For harmonic-oscillator (HO) wave functions, there is a lack in the suitability coming from the Gaussian fall-off behavior at large *r*, although it is analytically plausible to use [5, 6]. The two-frequency shell model approach using two HO size parameters were applied to exotic and stable nuclei with limited success [7]. The ground states in stable and unstable nuclei have been effectively studied using the Woods-Saxon (WS) potential WFs [8,9]. The approach to WFs is done through numerical solution for the radial Schrodinger problem. Nikiforov–Uvarov technique is a novel and promising method for solving a radial Schrodinger for the WS potential and other complicated forms [10,11, 12]. In addition, the properties of stable and exotic nuclei were extensively studied using transformed harmonic-oscillator (THO) WFs [13,14,15,16]. The theoretical outcomes utilizing THO WFs were encouraging and in excellent accord with empirical data. Utilizing the self-consistent mean-field WFs using Hartree-Fock with Sykrme forces is an additional approach [17,18,19]. Another useful tool for researching stable and unstable nuclei is the Cosh potent [20]. The Ginocchio potential was infrequently employed by Ginocchio(1984)[21], Ginocchio (1985)[22] and Coon and Jaqua (1991) [23] to investigate bulk characteristics of nuclei. The HO plus modified Bessel functions [24] and HO plus Hulthen-Weinberg WFs [25] have been successfully applied to both stable and exotic nuclei.

This work aims to study the ground charge densities, elastic electron scattering differential cross sections and elastic and inelastic form factors for ^{40,48}Ca isotopes. The radial WFs of THO in the local scaling transformation (LST) were used to study the different parity Coulomb transitions in ^{40}Ca and the same parity Coulomb transitions in ^{48}Ca. The nuclear shell approach with THO bases were harnessed. The HW [26] (with $1d_{3/2}1f_{7/2}$ subshells as a model space) and GXPF1 [27] (with fp model space) were used for ^{40}Ca and ^{48}Ca, correspondingly. The theoretical findings were compared to available empirical data.

2. Theory

In the formulation of LST, the radial WFs of THO is given by [13]

$$R^{TH0}_{nlj,n/p}(r) = \frac{f(r,\gamma_{n/p},m)}{r}\sqrt{\frac{df(r,\gamma_{n/p},m)}{dr}}\,R_{nl}\big(f\big(r,\gamma_{n/p},m\big),b_{n/p}\big) \quad (1)$$

where for single nucleon in Eq. (1) the quantum numbers are: n (principle quantum number), l (orbital quantum number), j (spin quantum number). The n/p represents the neutron/proton. In Equation (1), the scale function is given by (Karataglidis and Amos, 2005) [13].

$$f(r,\gamma_{n/p},m)=\left[\frac{1}{\left(\frac{1}{r}\right)^{m}+\left(\frac{1}{\gamma\sqrt{r}}\right)^{m}}\right]^{\frac{1}{m}} \tag{2}$$

For HO potential, their wave functions exhibit a Gaussian behavior ($e^{-\frac{r^2}{2b^2}}$). This characteristic is inconvenient to bulk properties of nuclei, because the radial WFs must behavior exponentially($e^{-\beta r}$) at r. To achieve such feature and diminish such deficiency, a LST is applied to the HO WF, the so-called transformed harmonic oscillator (THO) WFs. In the LST, the $r'=f(r)$ (new coordinate) is put instead of the previous coordinate $\vec{r}$ is . The function $f(r)$ or LST function or scaling function has the characteristic of being real, increasing, and subject to the conditions $f(0)=0$ and $f(\infty)=\infty$. Finally, the new WF is denoted by $R_{nl}^{THO}(r,b_{n/p})$ to differentiate it from $R_{nl}^{HO}(r,b_{n/p})$.

The derivative to scale function can be written as

$$\frac{df(r,\gamma_{n/p},m)}{dr}=\frac{-\left(\frac{1}{\left(\frac{1}{r}\right)^{m}+\left(\frac{1}{\gamma\sqrt{r}}\right)^{m}}\right)^{\frac{1}{m}}\left(-\frac{m\left(\frac{1}{r}\right)^{m}}{r}-\frac{m\left(\frac{1}{\gamma\sqrt{r}}\right)^{m}}{2r}\right)}{m\left(\left(\frac{1}{r}\right)^{m}+\left(\frac{1}{\gamma\sqrt{r}}\right)^{m}\right)} \tag{3}$$

The variables m and $\gamma_{n/p}$ in Eqs. (1) and (3) take integers and real numbers for m and $\gamma_{n/p}$, correspondingly. Both variables govern behavior of HO wave function shape in the asymptotic part.

For any nuclear species, the proton/neutron density distributions in pure configuration is derived from [5]:

$$\rho_{n/p}(r)=\frac{1}{4\pi}\sum_{nlj}\mathbb{O}_{nlj,n/p}\left|R_{nlj}^{THO}(r,b_{n/p})\right|^2 \tag{4}$$

The proton/neutron density distributions in mixing configuration is obtained from [5]:

$$\rho_{CJ,n/p}(r)=\frac{1}{\sqrt{4\pi}}\frac{1}{\sqrt{2J_i+1}}\sum_{ab}\mathcal{X}_{a,b,n/p}^{J_f\ J_i\ J}\left\langle j_a\middle\|Y_J\middle\|j_b\right\rangle R_{n_al_aj_a,n/p}^{THO}(r)R_{n_bl_bj_b,n/p}^{THO}(r) \tag{5}$$

In the equation above, The $\mathcal{X}_{a,b,n/p}^{J_f\ J_i\ J}$, represents the weight of the transition [28], which is yielded by the *Nushell* shell model code (Brown and Rae, 2007)[29]. The symbols a and b, stands for the quantum numbers of the single nucleon in the initial and final states, respectively. In Eq. (5), the J is the multipolarity of transition determined from selection rule. The density of nuclear charge is evaluated using the folding process for the proton and neutron densities, as follows [30,8]:

$$\rho_{ch}(r)=\rho_{ch,n}(r)+\rho_{ch,p}(r) \tag{6}$$

The size radii of the studied ^{40,48}Ca isotopes were calculated from (Elton and Swift, 1967) [8]:

$$\langle r^2\rangle_i^{1/2}=\sqrt{\frac{4\pi}{i}\int_0^{\infty}\rho_i(r)r^4dr} \tag{7}$$

the letters *i* in the above equation stand for protons, neutrons, and nucleons.

In the Born approximation, the longitudinal form factor for the scattering of electrons in the first order is provided by [28, 31]:

$$F_{J,ch}^{C}(q) = \frac{1}{Z}\sqrt{\frac{4\pi}{(2J_i+1)}}\sum_{n/p}\langle J_f \| \boldsymbol{O}_J^C(q,n/p) \| J_i \rangle \, f_{n/p}(q) \tag{8}$$

In Eq. (8), the longitudinal transition operator is [28]:

$$\boldsymbol{O}_{JM_J}^{C}(q,n/p) = \int j_J(qr)\, Y_{JM_J}(\Omega_r)\hat{\rho}_{n/p}(\vec{r})d\vec{r} \tag{9}$$

The density operator $\hat{\rho}_{n/p}(\vec{r})$), spherical harmonic oscillator ($Y_{JM_J}(\Omega_r)$, and spherical Bessel function $(j_J(qr)$ are described in detail by Arfken et al.(2013) [32].

The relationship between single nucleon matrix elements and many-nucleon matrix elements in Eq. (8) is [28]:

$$\langle J_f \| \boldsymbol{O}_J^C(q,n/p) \| J_i \rangle = \sum_{ab} X_{a,b,p/n}^{J_i,J_f,J} \, \langle b,n/p \| O_J^C(q,r,t_z) \| a,n/p \rangle \tag{10}$$

The $\chi_{a,b,n/p}^{J_f \; J_i \; J}$ in the above equation denotes the weight of transition, evaluated from *Nushell* shell model code [28].

$$\chi_{a,b,n/p}^{J_i,J_f,J} = \frac{\left\langle J_f \middle| \left| \left[c_{b,t_z}^{+} \otimes \tilde{c}_{a,t_z} \right]^J \right| \middle| J_i \right\rangle}{\sqrt{2J+1}} \tag{11}$$

In isospin formalism, the $\chi_{a,b,n/p}^{J_i,J_f,J}$ in Eq. (11) can be written as

$$\chi_{a,b,p/n}^{J_i,J_f,J} = (-1)^{T_f - T_Z}\left(\sqrt{2}\begin{pmatrix} T_f & 0 & T_i \\ -T_Z & 0 & T_Z \end{pmatrix}\frac{\chi_{\alpha,\beta}^{\Gamma_i,\Gamma_f,(J,T=0)}}{2} \right.$$
$$\left. +/-\sqrt{6}\begin{pmatrix} T_f & 1 & T_i \\ -T_Z & 0 & T_Z \end{pmatrix}\frac{\chi_{\alpha,\beta}^{\Gamma_i,\Gamma_f,(J,T=1)}}{2} \right) \tag{12}$$

where $\chi_{\alpha,\beta}^{\Gamma_i,\Gamma_f,(J,T=0)}$ is the weight of transition in isospin formalism.

The Coulomb form factor for any multipolarity J was accounted by:

$$F_{J,ch}(q) = \frac{4\pi}{Z}\int_0^{\infty} j_J(qr)\rho_{J,ch}(r)r^2 dr \tag{13}$$

For $J = 0$, the charge form factor is Fourier transform to the ground state distribution of charge. With the Born plane wave approximation, the scattering cross-section of scattered electrons can be expressed in terms of the square of charge form factor [8]:

$$\left(\frac{d\sigma}{d\Omega}\right)_{exp.} = \left(\frac{d\sigma}{d\Omega}\right)_{Mott} \left|F_J(q)\right|^2 \tag{14}$$

The $\left(\frac{\mathrm{d}\sigma}{\mathrm{d}\Omega}\right)_{\mathrm{Mott}}$ stands for the elastic relativistic scattering cross section of electrons from a point nucleus. The $\left(\frac{\mathrm{d}\sigma}{\mathrm{d}\Omega}\right)_{\mathrm{Mott}}$ gives the relationship between the scattering angle and the energy of the incident electron, and is based on the Coulombic interaction between the electron and the nucleus:

$$\left(\frac{d\sigma}{d\Omega}\right)_{Mott} = \frac{Z^2\alpha^2(\hbar c)^2}{4E^2\, sin^4\left(\frac{\theta}{2}\right)}\left[1 - \beta^2\, sin\left(\frac{\theta}{2}\right)\right] \tag{15}$$

where $\beta = \frac{v}{c}$ is Lorentz factor.

For inelastic Coulomb transitions ($J \neq 0$) with different parities, the selection rule becomes, $\pi_i . \pi_f = (-1)^{J+1}$. In Eq. (13), the transition density of charge $\rho_{J,ch}(r)$ is separated into two parts: one for the model space and the other by the core polarization (CP) [22], i.e.,

$$\rho_{ch,J}(r) = \rho^{MS}_{ch,J}(r) + \rho^{CP}_{ch,J}(r) \quad (16)$$

The $\rho^{CP}_{ch,J}(r)$ in Eq. (16) is evaluated using Tassie [33], Bohr-Mottelson [34] models and valence model [28] as follows:

$$\rho^{CP,T}_{ch,J}(r) = N_T r^{J-1} \frac{d}{dr}\rho_{ch}(r) \quad (17)$$

$$\rho^{CP,B-M}_{ch,J}(r) = N_{B-M} \frac{d}{dr}\rho_{ch}(r) \quad (18)$$

and

$$\rho^{CP,V}_{ch,J}(r) = N_V \rho_{ch}(r) \quad (19)$$

The above CP methods are used to include the effect $\rho^{CP}_{ch,J}(r)$ in Eq. (16).

The *N*'s constants in Eq. (17), (18) and (19) were fixed to reproduce the experimental reduced transition probabilities. Finally, the $\rho^{MS}_{J,ch,t_z}(r)$ in Eq (16) were obtained from shell model calculations using Nushell code for active nucleons within the assigned model spaces [5].

3. Results and discussion

The current theoretical calculations were mainly based on using shell model approach. The nuclear shell model *Nushell* code was run to yield the values of $\chi^{J_i,J_f,J}_{a,b,n/p}$ necessary to initiate the theoretical calculations. The distinctive addition to the theory of the work is the use of the basis of THO WFs instead of HO potential. Such addition is important to improve the behaviour of HO WFs at large *r*. For ^{40}Ca, the HW interaction was chosen with $1d_{3/2}1f_{7/2}$ subshells as a model space; the core is ^{32}S. For ^{48}Ca, the GXPF1 interaction was opted with $1f_{7/2}2p_{3/2}1f_{5/2}\ 2p_{1/2}$ subshells as a model space; The core is ^{40}Ca. the THO basis in parallel with the OBDMEs of HW and GXPF1 interactions, the charge densities, elastic electron scattering differential cross sections, and elastic and inelastic Coulomb form factors were searched.

For ^{40}Ca, the adjusted occupancies for protons over subshells were as follows: $\mathbb{O}_{1s_{1/2},p} = 2$, $\mathbb{O}_{1p_{3/2},p} = 3$, $\mathbb{O}_{1p_{1/2},p} = 2$, $\mathbb{O}_{1d_{5/2},p} = 6$, $\mathbb{O}_{1d_{3/2},p} = 4$, $\mathbb{O}_{2s_{1/2},p} = 1$, $\mathbb{O}_{1f_{7/2},p} = 2$. For ^{48}Ca, the adjusted occupancies were $\mathbb{O}_{1s_{1/2},p} = 1.2$, $\mathbb{O}_{1p_{3/2},p} = 3$, $\mathbb{O}_{1p_{1/2},p} = 2$, $\mathbb{O}_{1d_{5/2},p} = 5$, $\mathbb{O}_{1d_{3/2},p} = 3.4$, $\mathbb{O}_{2s_{1/2},p} = 1.2$, $\mathbb{O}_{1f_{7/2},p} = 3.2$, $\mathbb{O}_{1p_{3/2},p} = 1$.

Such occupancies were used to initiate the present calculations.

In Table 1, the parameters of total initial spin (J) quantum numbers, total initial isospin (T) quantum numbers, parity, and b_p ,m and γ_p of THO wave functions were displayed. The values of b_p , m and γ_p were fixed to recreate the empirical size radii for ^{40,48}Ca isotopes.

In Table 2, the experimental [35] and calculated rms proton and charge radii were tabulated. With the fixed parameters in Table 1, the theoretical findings were in very good match with empirical data.

The computed excitation energies using HW and GXPF1 were shown and compared with available empirical findings in Table 3. It is obvious that the computed energy levels for the studied transition were in good match with corresponding empirical data [36].

The evaluated and empirical charge densities were portrayed in Figure 1 for ^{40}Ca (a) and ^{48}Ca (b), correspondingly. The solid curves represent the theoretical results using THO WFs

with adjusted occupancies for ^{40}Ca (a) and ^{48}Ca (b). The filled dotted symbols represent experimental results. From the depicted results, it is clear that the theoretical results were in excellent match with experimental data [36,37].

Elastic charge structure factors for ^{40}Ca (a) and ^{48}Ca (b) were drawn. The computed results were represented by the solid curves, while the dotted filled circles represent the experimental data. As it is shown from the graphs that the calculations were in good agreement with empirical findings; at small q, there was a slight difference between theoretical and empirical results while at large q, there was slight underestimation in the calculations.

In Figure 3, the graphs (a) for ^{40}Ca and (b) for ^{48}Ca represent the theoretical and empirical elastic electron scattering differential cross-sections at the (E=250 MeV) represented by solid curves for theoretical calculations and dotted filled circles for experimental data [38]. The calculated results were very good match with experimental data at small and middle θ, while at very large θ values there were slight differences.

Figure 4 shows the experimental and calculated inelastic charge structure factor for ^{40}Ca using shell model with THO basis for the different parity transitions: $(a)\ 0^+ \rightarrow 3_1^-\ (E_x = 3.74\ MeV)$, $(b)\ 0^+ \rightarrow 3_2^-\ (E_x = 6.29\ MeV), (c)\ 0^+ \rightarrow 3_3^-\ (E_x = 6.59\ MeV)$, $and\ (d)\ 0^+ \rightarrow 5_1^-\ (E_x = 4.49\ MeV)$. The experimental data were represented by the dotted circles [36], while the solid, dashed, and dashed-dotted curves represent the theoretical results with the inclusion of CP effect using the B-M, the T and the V models, respectively. it is clear from the four graphs that the B-M model were well described that experimental data for $(a)\ 0^+ \rightarrow 3_1^-\ (E_x = 3.74\ MeV)$ and $(d) 0^+ \rightarrow 5_1^-\ (E_x = 4.49\ MeV)$, while the transition in $(b)\ 0^+ \rightarrow 3_2^-\ (E_x = 6.29\ MeV)$ was well described by T model. Finally, all CP models for the transition in $(c)\ 0^+ \rightarrow 3_3^-\ (E_x = 6.59\ MeV)$ was in poor match with empirical data.

Figure 5 shows the experimental and calculated inelastic charge structure factors using the shell model using THO basis for 48Ca for the same parity transitions: $(a)\ 0^+ \rightarrow 2_1^+\ (E_x = 3.841\ MeV), (b)\ 0^+ \rightarrow 2_2^+\ (E_x = 9.29MeV)\ (c)\ 0^+1 \rightarrow 4_2^+\ (E_x = 6.34\ MeV)$. The experimental data were represented by the filled circles [37], while the solid, dashed, and dashed-dotted curves represent the inclusion of CP effect using the B-M, the T and the V models, respectively. It is obvious that the results of B-M model were in very good match with empirical data for the transitions in $(a)\ 0^+ \rightarrow 2_1^+\ (E_x = 3.841\ MeV)$, $(b)\ 0^+ \rightarrow 2_2^+\ (E_x = 9.29MeV)$, $(c)\ 0^+1 \rightarrow 4_2^+\ (E_x = 6.34\ MeV)$. all CP models had poor behaviour to reproduce the experimental finding. It is worth mentioning that with the dominance of small deformation, the Bohr-Mottelson elucidate the laboratory data unlike Tassie and valence models which success in nuclei with large deformation, i.e., the Tassie model. The ^{40,48}Ca nuclei are even-even nuclear samples, therefore, one expects small deformations due to high stability of such nuclei. The poor results of valence and Tassie models is due to such small deformation.

Table1: Total spin, isospin, and the parameters of THO

$^{A}_{Z}X_N$	$J^{\pi}T$ [36][37]	b_p	m	γ_p
$^{40}_{20}Ca_{20}$	0^+0	1.891	8	3.028
$^{48}_{20}Ca_{28}$	0^+0	1.845	8	3.019

Table2: Evaluated rms neutron, proton, matter radii, and charge for $^{40}_{20}Ca_{20}$ and $^{48}_{20}Ca_{28}$ nuclei

$^{A}_{Z}X_N$	$\langle r_{ch}^2\rangle^{1/2}$	Exp. $\langle r_{ch}^2\rangle^{1/2}$ [35]	$\langle r_p^2\rangle^{1/2}$
$^{40}_{20}Ca_{20}$	3.450	3.482(25)	3.374
$^{48}_{20}Ca_{28}$	3.459	3.470	3.390

Table 3: Empirical and Calculated energy levels for 40,48Ca isotopes,

${}^{A}_{Z}X_{N}$	$J_i^+T \rightarrow J_f^+T$ [36][37]	Calculated $E_x(MeV)$	Empirical $E_x(MeV)$
${}^{40}_{20}Ca_{20}$	$0^+ \rightarrow 3_1^-$	4.164	3.74
	$0^+ \rightarrow 3_2^-$	7.633	6.29
	$0^+ \rightarrow 3_3^-$	9.683	6.59
	$0^+ \rightarrow 5_1^-$	4.934	4.49
${}^{48}_{20}Ca_{28}$	$0^+ \rightarrow 2_1^+$	3.791	3.831
	$0^+ \rightarrow 2_2^+$	6.397	2.29
	$0^+ \rightarrow 4_2^+$	6.006	6.34

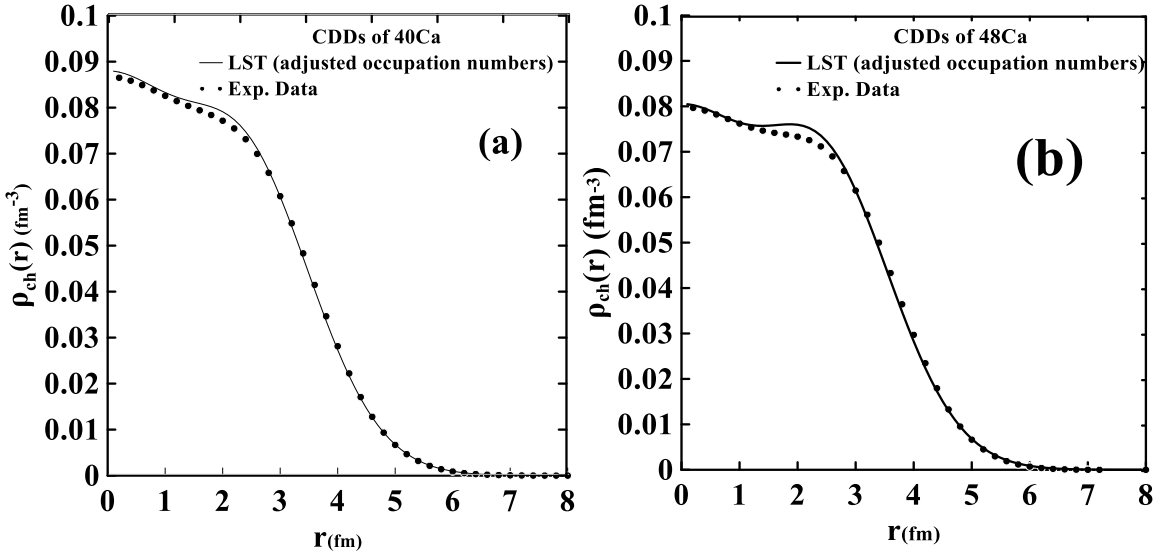

Figure 1: CDDs calculated by adjusted occupancies for ^{40}Ca (a), and ^{48}Ca (b) are represented by the solid curve compared with data represented by dotted circles symbols taken from Vries, Jager and Vries (1987) [35]

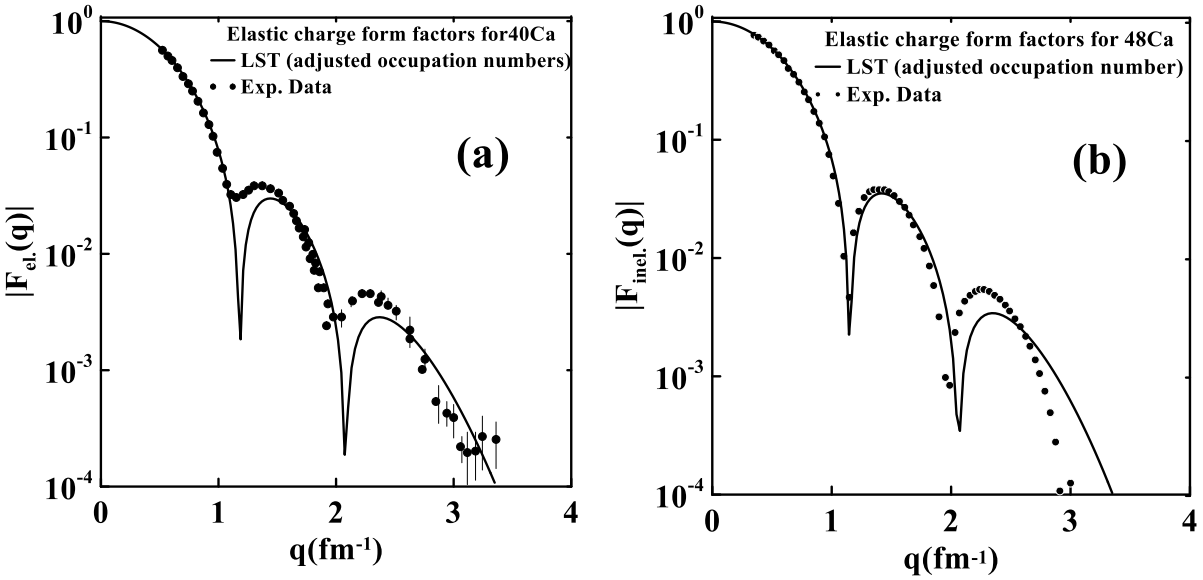

Figure 2: Calculated elastic charge form factor for ^{40}Ca (a), and ^{48}Ca(b) are represented by the solid curves. The filled dotted circles represent the experimental data, which were taken from Sinha et al.(1973) [39] and Wise et al.(1985) [37].

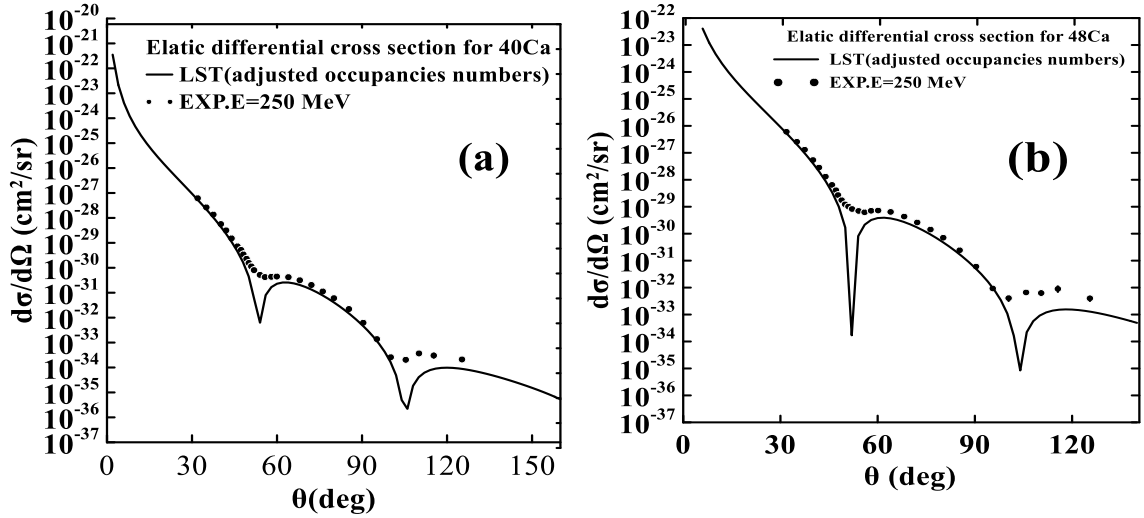

Figure 3: calculated elastic differential the cross section for, ^{40}Ca (a), and ^{48}Ca (b) at E=250MeV are represented by the solid curve. The filled dotted circles represent the experimental data, which were taken from Frosch, Hofstadter, Mccarthy et al.(1968) [38].

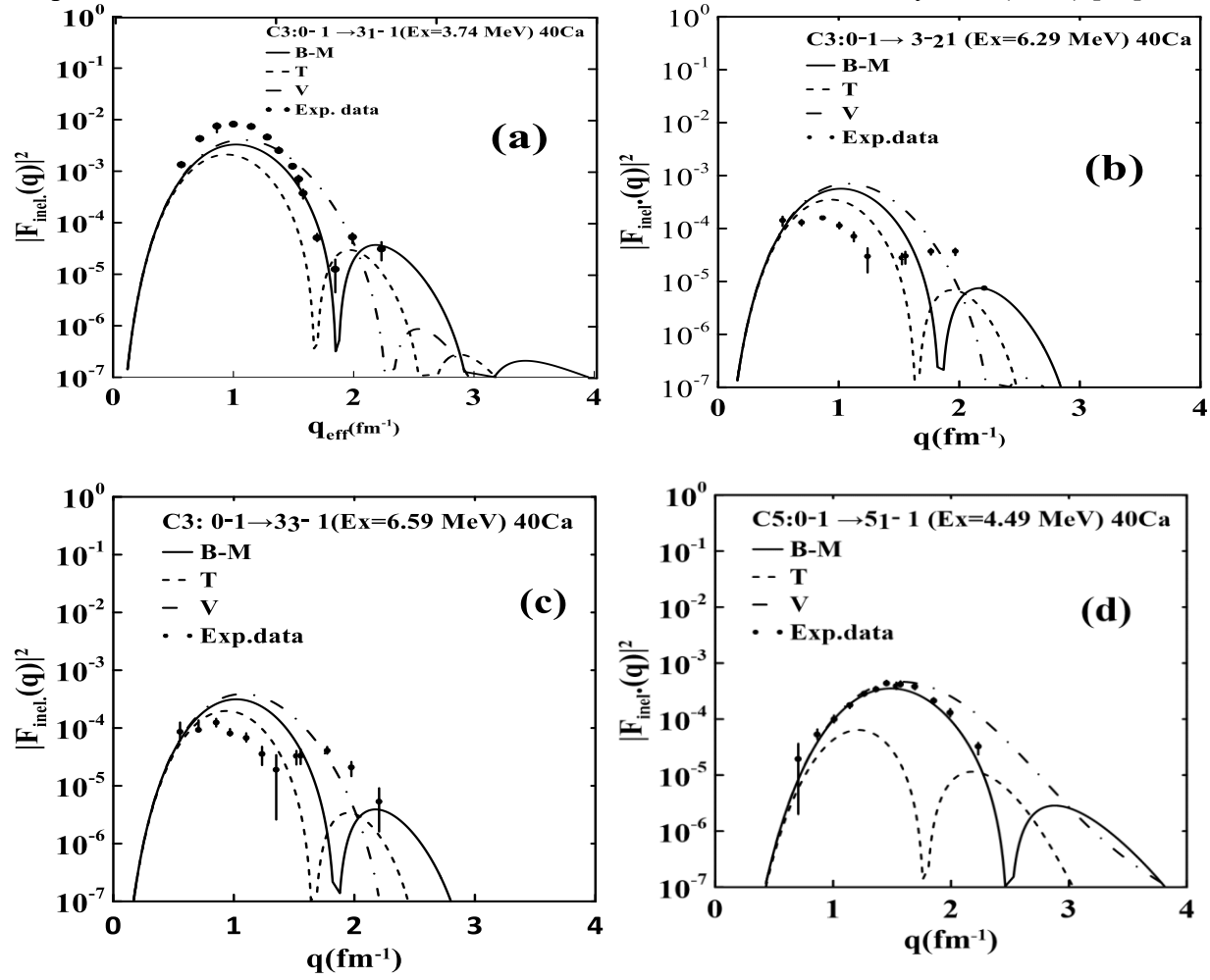

Figure 4: Calculated data for Inelastic transitions related to form factors to the C3 and C5 for the ^{40}Ca $(a)\ 3_1^-,\ (b)\ 3_2^-, (c)\ 3_3^-,\ and (d)\ 5_1^-$. The theoretical results were computed using Bohr-Mottelson, valence, and Tassie models represented by solid, dashed-dotted, and dashed curves. The experimental data were represented by dotted circles symbols taken Itoh, Oyamada and Torizuka (1970) [36].

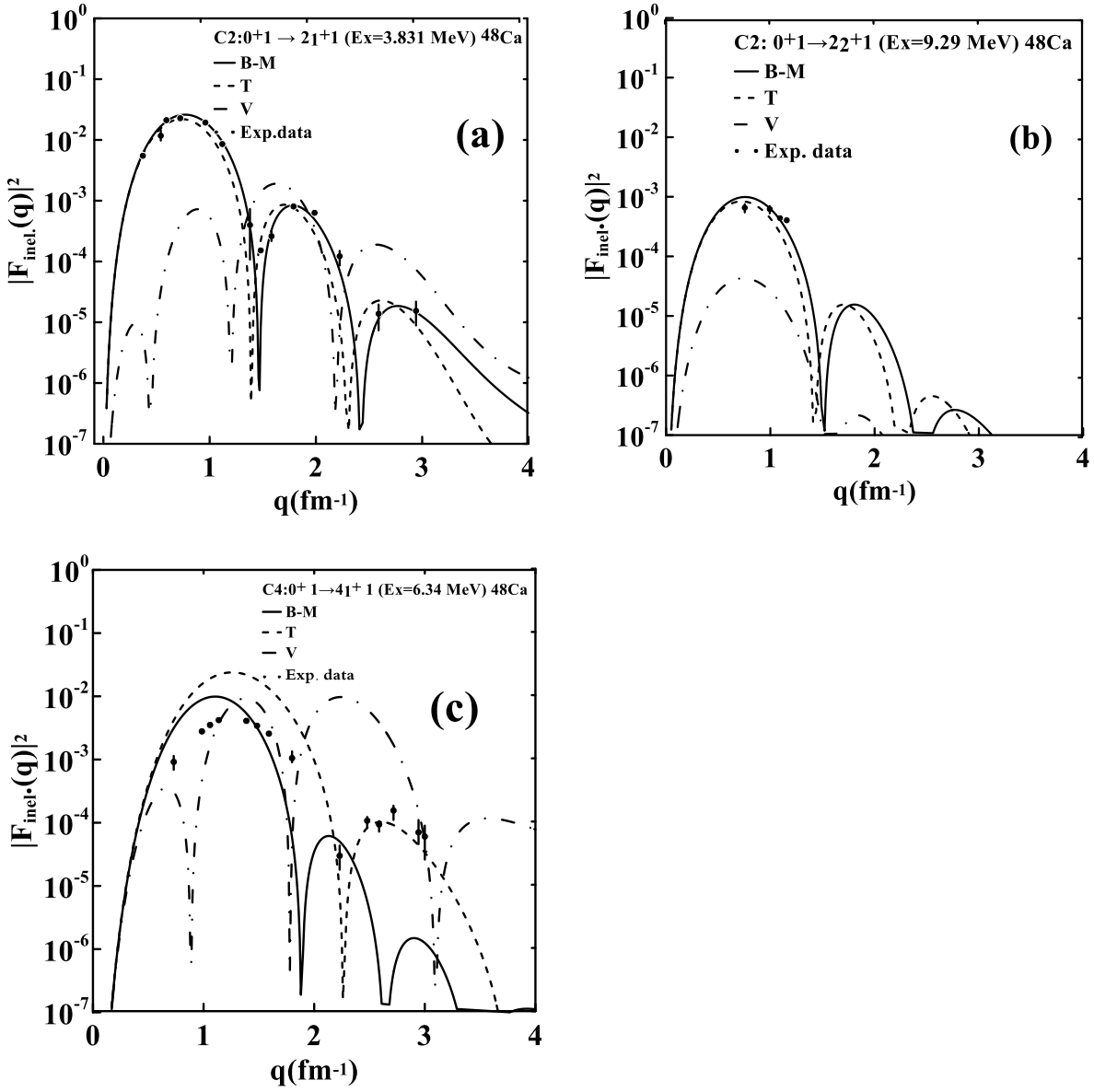

Figure 5: Calculated data for Inelastic transitions related to form factors to the C2 and C4 for the ^{48}Ca $(a)\ 2_1^+$, $(b)\ 2_2^+$, $and (c) 4_1^+$. The results were computed using valence, Tassie, and Bohr-Mottelson models represented by dashed-dotted, dashed, and solid curves, correspondingly. The experimental data were represented by dotted circles symbols from Wise et al. (1985) [37].

3. Conclusion

The elastic and inelastic Coulomb multipoles for the different and for the same parity transitions were searched for ^{40,48} Ca. For ^{40}Ca, the three different parity transitions: $0^+ \rightarrow 3_1^-$ $(E_x = 3.74\ MeV)$, $0^+ \rightarrow 3_2^-$ $(E_x = 6.29\ MeV)$ and $0^+ \rightarrow 3_3^-$ $(E_x = 6.59\ MeV)$ in parallel with C5 transitions, $0^+ \rightarrow 5_1^-$ $(E_x = 4.49\ MeV)$ were searched. For ^{48}Ca, the two same parity C2 transitions: $0^+ \rightarrow 2_1^+$ $(E_x = 3.841\ MeV)$ and $0^+ \rightarrow 2_2^+$ $(E_x = 9.29 MeV)$ in parallel with C4 transitions $0^+1 \rightarrow 4_2^+$ $(E_x = 6.34\ MeV)$ were investigated. The theory of the present work was based on shell model approach using HW and GXPF1 interactions for ^{40}Ca and ^{48}Ca, respectively. the basis of THO in the LST were applied to evaluate the charge densities, differential cross sections, and elastic and inelastic form factors. The model space for ^{40}Ca in the HW interaction is $1d_{3/2}1f_{7/2}$ subshells while for ^{48}Ca in the GXPF1 interaction, the model

space is fp-shell. With the inclusion of THO, the computed charge densities and electron scattering differential cross sections were in very good match with empirical data. Finally, the inclusion of the CP effects improved the outcome of the computed inelastic Coulomb form factors were greatly enhanced. In general, the results of Bohr-Mottelson model possess acceptability more than Tassie and valence models for ^{40,48} Ca which have small deformation on contrary to Tassie model which is successful in nuclei with large deformation. The poor agreement of results of valence model is attributed to its simple mathematical form. It is recommended to enlarge the model space of nucleon in the valence in presence of more sophisticated computers for such run.

References

[1] A. N. Antonov, P. E. Hodgson, and I. Z. Petkov, "*Nucleon Momentum and Density Distributions in Nuclei*". Clarendon Press, 1988.

[2] J. D. Walecka, "*Electron Scattering for Nuclear and Nucleon Structure*". Cambridge University Press, 2023.

[3] C. J. Batty, E. Friedman, H. J. Gils, and H. Rebel, "Experimental Methods for Studying Nuclear Density Distributions," *Adv. Nucl. Phy.*, Springer US, pp. 1–188, 1989.

[4] C. A. Bertulani, *Nuclear Physics in a Nutshell*. Princeton University Press, 2007.

[5] R. A. Radhi, A. K. Hamoudi, and A. R. Ridha, "Elastic Electron Scattering From Unstable Neutron-Rich ^{19}C Exotic Nucleus," *Iraqi J. Sci.*, vol. 54, no. 2, pp. 324–332, 2013.

[6] S. S. Mashaan, F. Z. Majeed, "Inelastic longitudinal electron scattering C2 form factors in ^{48}Ca nucleus by using sigma meson as a residual interaction Research," *Iraqi J. Sci.*, vol. 55, pp. 151–160, 2014.

[7] A. K. Hamoudi, R. A. Radhi, and A. R. Ridha, "Theoretical study of matter density distribution and elastic electron scattering form factors for the neutron-rich ^{22}C exotic nucleus," *Iraqi J. Phys.*, vol. 10, pp. 25–34, 2012.

[8] L. R. B. Elton and A. Swift, "Single-particle potentials and wave functions in the 1p and 2s-1d shells," *Nucl. Phys. A*, vol. 94, no. 1, pp. 52–72, 1967.

[9] S. Gamba, G. Ricco, and G. Rottigni, "A phenomenological woods-saxon potential for p-shell nuclei," *Nucl. Phys. A*, vol. 213, pp. 383–396, 1973.

[10] V. H. Badalov, H. I. Ahmadov, and A. I. Ahmadov, "Analytical Solutions of The Schrodinger Equation With The Woods Saxon Potential For Arbitrary l State," *Int. J. Mod. Phys. E*, vol. 18, no. 3, pp. 631–641, 2009.

[11] M. R. Pahlavani and S. A. Alavi, "Study of nuclear bound states using mean-field woods saxon and spin-orbit potentials," *Mod. Phys. Lett. A*, vol. 27, no. 29, pp. 1–13, 2012.

[12] E. Yazdankish, "Solving of the Schrodinger Equation Analitically with an Approximated Scheme of the Woods-Saxon Potential by the Systematically Method of Nikiforov- Uvarov," *Int. J. Mod. Phys. E*, vol. 29, 2050032, pp. 1-14, 2020.

[13] S. Karataglidis and K. Amos, "Local scale transformations and extended matter distributions in nuclei," . *Phys. Rev. C*, vol. 064601, pp. 1–13, 2005.

[14] S. H. Mohammed and A. R. Ridha, "Study of nuclear structure for carbon isotopes using local scale transformation technique in shell model," *Iraqi J. Phys.*, vol. 16, no. 39, pp. 103–116, 2019.

[15] S. H. Mohammed and A. R. Ridha, "Theoretical study of the electromagnetic structure of boron isotopes using local scale transformation technique," *Iraqi J. Sci.*, vol. 59, no. 4, pp. 1866–1877, 2018.

[16] H. F. Ojaimi and A. R. Ridha, "Study of Inelastic Coulomb Form Factors in 18O using the Radial Wave functions of Transformed Harmonic-Oscillator," in *2022 International Congress on Human-Computer Interaction, Optimization and Robotic Applications (HORA)*, IEEE, pp. 1–6, 2022.

[17] W. Zuheir and A. R. Ridha, "Investigation of the Ground State Nuclear Density Distributions of Unstable ^{17,18,19,20}F Isotopes," *Indian J. Nat. Sci.*, vol. 8, no. 44, pp.12733-12744, 2017.

[18] X. Guo, Z. Wang, T. Li, and J. Liu, "Calculation of charge form factor of elastic electron scattering based on Skyrme force and relativistic eikonal approximation," *Int. J. Mod. Phys. E*, vol. 28, no. 3 pp. 1-15, 2019.

[19] L. Tong and S. Yan, "Real space density-constrained time-dependent Hartree-Fock-Bogoliubov method and pairing effects in the fusion of calcium isotopes," *Phys. Rev. C*, vol. 105, pp. 14613, 2022.
[20] S. S. Odah and A. R. Ridha, "Investigation of Ground Density Distributions and Charge Form Factors for ^{14,16,18,20,22}N using Cosh Potential," *Iraqi J. Sci.*, vol. 63, no. 9, pp. 3737–3745, 2022.
[21] J. N. Ginocchio, "A class of exactly solvable potentials. I. One-dimensional Schrödinger equation," *Ann. Phys. (N. Y).*, vol. 152, no. 1, pp. 203–219, 1984.
[22] J. N. Ginocchio, "A class of exactly solvable potentials II. The three-dimensional Schrödinger equation," *Ann. Phys. (N. Y).*, vol. 159, no. 2, pp. 467–480, 1985.
[23] S. A. Coon and L. Jaqua, "Wave function efFects and the elastic magnetic form factor of '17O," *Phys. Rev. C*, vol. 44, no. 1, pp. 203–208, 1991.
[24] S.-A. J. Khalaf and A. R. Ridha, "Ground state properties of Beryllium isotopes using the radial wave functions of harmonic-oscillator and modified Bessel functions," in *AIP Conf. Proc.*, vol. 2922, no. 1, no. 090005, pp. 1-8, 2024.
[25] A. M. Hameed and A. R. Ridha, "Ground State Structure of Helium and Phosphorus Isotopes using the Radial Wave Functions of Harmonic-Oscillator and Hulthen Potentials," *Iraqi J. Sci.*, vol. 64, no. 5, pp. 2250–2260, 2023.
[26] S. T. Hsieh, X. Ji, R. Mooy, and B. H. Wildenthal, "Analysis of features in the A=34–48 region in terms of d3/2 and f7/2 degrees of freedom," in *AIP Conference Proceedings*, AIP, vol. 142, pp. 357–375. 1986.
[27] M. Honma, T. Otsuka, B. A. Brown, and T. Mizusaki, "Effective interaction for pf-shell nuclei," *Phys. Rev. C - Nucl. Phys.*, vol. 65, no. 061301, pp.1-5 2002.
[28] B.A. Brown and B.H. Wildenthal, C. F. Williamson, F. N. Rad, and S. Kowalski, Hall Cranneland Hall Crannel, "Shell-model analysis of high-resolution data for elastic and inelastic electron scattering on ^{19}F," *Phys. Rev. C*, vol. 32, no. 4, pp. 1127–1156, 1985.
[29] B. A. Brown and W. D. M. Rae, "Nushell @ MSU, MSU-NSCL report," pp. 1–34, 2007.
[30] H. Chandra and G. Sauer, "Relativistic corrections to the elastic electron scattering from 208pb," *Phys. Rev. C*, vol. 13, pp. 245-252, 1976.
[31] R. F. Frosch, R. Hofstadter, J. S. Mccarthy, G. K. N6ldeke,t k. J. Van oostrum and m. R. Yearian, "Electron scattering and nuclear structure," *Adv. Phys.*, vol. 15, no. 57, pp. 1–109, 1966.
[32] G. B. Arfken, H. J. Weber, and F. E. Harris, *Mathematical Methods for Physicists: A Comprehensive Guide*. Elsevier Science, 2013.
[33] A. N. Bohr and B. R. Mottelson, *Nuclear Structure (in 2 volumes)*. World Scientific Publishing Company, 1998.
[34] J. A. M. W. Greiner, *Nuclear Models*. Springer-Verlag Berlin Heidelberg New York, 1996.
[35] H. D. E. Vries, C. W. D. E. Jager, and C. D. E. Vries, "Charge-Density-Distribution Parameters from Elastic Electron Scattering," *At. Data Nucl. Data Tables*, vol. 36, no. 3, pp. 495-536, 1987.
[36] K. Itoh, M. Oyamada, and Y. Torizuka, "Study of nuclear states in Ca40 by inelastic electron scattering," *Phys. Rev. C*, vol. 2, pp. 2181–2199, 1970.
[37] J. E. Wise , J. S. McCarthy, R. Altemus, B.E. Norum, and R. R. Whitney, "Inelastic electron scattering from Ca48," *Phys. Rev. C*, vol. 31, pp. 1699-1714, 1985.
[38] R. F. Frosch *et al.*, "Electron Scattering Studies of Calcium and Titanium Isotopes," *Phys. Rev.*, vol. 174, no. 4, pp. 1380–1399, 1968.
[39] B. B. P. Sinha, G. A. Peterson, R. R. Whitney, I. Sick, and J. S. McCarthy, "Nuclear charge distributions of isotone pairs. II. K39 and Ca40," *Phys. Rev. C*, vol. 7, pp. 1930-1938 1973.